New Journal of Physics
The open access journal at the forefront of physics

Deutsche Physikalische Gesellschaft DPG IOP Institute of Physics

PAPER • OPEN ACCESS

Light-induced anomalous Hall effect in massless Dirac fermion systems and topological insulators with dissipation

To cite this article: S A Sato *et al* 2019 *New J. Phys.* **21** 093005

View the article online for updates and enhancements.

IOP ebooks™

Bringing you innovative digital publishing with leading voices to create your essential collection of books in STEM research.

Start exploring the collection - download the first chapter of every title for free.

This content was downloaded from IP address 131.169.224.158 on 13/09/2019 at 10:24

New Journal of Physics
The open access journal at the forefront of physics

Deutsche Physikalische Gesellschaft DPG
IOP Institute of Physics

Published in partnership with: Deutsche Physikalische Gesellschaft and the Institute of Physics

OPEN ACCESS

RECEIVED
31 May 2019

REVISED
22 July 2019

ACCEPTED FOR PUBLICATION
13 August 2019

PUBLISHED
4 September 2019

Original content from this work may be used under the terms of the Creative Commons Attribution 3.0 licence.

Any further distribution of this work must maintain attribution to the author(s) and the title of the work, journal citation and DOI.

PAPER

Light-induced anomalous Hall effect in massless Dirac fermion systems and topological insulators with dissipation

S A Sato[1,2], P Tang[2], M A Sentef[2], U De Giovannini[2], H Hübener[2] and A Rubio[2,3]

[1] Center for Computational Sciences, University of Tsukuba, 1-1-1 Tennodai, Tsukuba, Ibaraki 305-8577, Japan
[2] Max Planck Institute for the Structure and Dynamics of Matter, Luruper Chaussee 149, D-22761 Hamburg, Germany
[3] Center for Computational Quantum Physics (CCQ), The Flatiron Institute, 162 Fifth Avenue, New York, NY 10010, United States of America

E-mail: ssato@ccs.tsukuba.ac.jp **and** angel.rubio@mpsd.mpg.de

Keywords: Floquet states, open quantum systems, anomalous Hall effect

Abstract

Employing the quantum Liouville equation with phenomenological dissipation, we investigate the transport properties of massless and massive Dirac fermion systems that mimics graphene and topological insulators, respectively. The massless Dirac fermion system does not show an intrinsic Hall effect, but it shows a Hall current under the presence of circularly-polarized laser fields as a nature of a optically-driven nonequilibrium state. Based on the microscopic analysis, we find that the light-induced Hall effect mainly originates from the imbalance of photocarrier distribution in momentum space although the emergent Floquet–Berry curvature also has a non-zero contribution. We further compute the Hall transport property of the massive Dirac fermion system with an intrinsic Hall effect in order to investigate the interplay of the intrinsic topological contribution and the extrinsic light-induced population contribution. As a result, we find that the contribution from the photocarrier population imbalance becomes significant in the strong field regime and it overcomes the intrinsic contribution. This finding clearly demonstrates that intrinsic transport properties of materials can be overwritten by external driving and may open a way to ultrafast optical-control of transport properties of materials.

1. Introduction

Controlling material properties by external driving is one of the ultimate goals of modern condensed matter physics. Light is one of the most important drivers to realize ultrafast control of material properties [1, 2]. A strong terahertz field can couple with a specific phonon mode in solids and largely populate the phonon mode. As a result of the significant phonon excitation, electron–phonon coupling is renormalized, and a superconducting state is realized in the picosecond time scale [3, 4]. Furthermore, recently it was theoretically demonstrated that an optically-driven phonon can induce magnetism in two-dimensional materials [5]. An intense infrared laser field can strongly couple also with electrons in solids and significantly renormalize electronic structures within a optical cycle. The light-induced modulation of electronic structure in solids has been suggested theoretically as a means to modify effective interactions [6–10] and possibly tune between competing phases of strongly correlated electron systems [11–13]. On sub-femtosecond time scales, even subcycle electron dynamics in solids can now be investigated with attosecond experimental techniques towards petahertz optoelectronics [14–17].

In contrast to the subcycle electron dynamics in solids, the cycle-averaged dynamics is another important subject and has been intensively studied in a number of theoretical works in terms of Floquet theory [18–24], where Floquet states $|\Psi^{\mathrm{F}}\rangle$ are stationary solutions of Schrödinger equation with a time-periodic Hamiltonian, $H(t) = H(t + T)$. In a seminal work by Oka and Aoki [18], it was theoretically demonstrated that the topology of condensed-matter systems can be controlled by light via the Floquet engineering. Furthermore, based on the emergence of topology, the light-induced anomalous Hall effect in graphene, analogous to the Haldane model

© 2019 The Author(s). Published by IOP Publishing Ltd on behalf of the Institute of Physics and Deutsche Physikalische Gesellschaft

[25] with broken time-reversal symmetry [26], has been predicted. Motivated by this theoretical prediction, McIver *et al* recently observed the light-induced anomalous Hall effect in graphene under the presence of a circular laser field [27]. Soon after, we have theoretically investigated the microscopic origin of the observed light-induced anomalous Hall effect by the quantum Liouville equation with phenomenological dissipation [28]. As a result, we clarified that the imbalance of photocarrier distribution of topological Floquet states in the Brillouin zone predominantly causes the light-induced anomalous Hall current with a small contribution from the emergent Berry curvature of the Floquet states.

The anomalous Hall effect induced by circularly polarized light has been heavily discussed in various theoretical works [18, 29–34] from the point of view of intrinsic and light-induced Berry curverture contributions in order to explore a possibility of diagnosing and steering topological properties by light. However, despite the great interest in the subject, population effects with dissipation have only recently been discussed more seriously in the context of Floquet and topological engineering in open [35, 36] and closed [37–39] nonequilibrium many-body systems. Dissipation and population effects are definitely important in explaining the recent experiments on the light-induced Hall effect [27, 28], and here we will provide an in-depth discussion of them. In this work, we first discuss appropriate treatment of phenomenological relaxation for dissipative light-driven condensed matter systems, taking care of electronic decoherence and thermalization via electron–electron and electron–phonon scattering. Then, we investigate the light-induced anomalous Hall effect in a massless Dirac fermion system as a model of graphene and elucidate the population contribution and the topological contribution to the Hall effect. Finally, we investigate the light-induced anomalous Hall effect in a massive Dirac fermion system as a simple model describing a topological insulator in order to explore the interplay of the intrinsic topological contribution and the extrinsic light-induced contribution to the Hall current. As a result, we find that the intrinsic contribution can be weakened by strong optical driving and the extrinsic contribution dominates the properties of the driven system in the strong field regime. These findings indicate robustness and generality of the photocarrier population effect and open a possibility to control of material properties via population-control on top of state-control by light.

This paper is organized as follows: in section 2 we describe the theoretical modeling of massless and massive Dirac fermion systems with the phenomenological relaxation. In section 3 we first assess phenomenological relaxation constructed with two kinds of physical basis sets: one is the static Bloch state, and the other is the dynamical Houston state. Then, we investigate the Hall transport property of massless and massive Dirac fermion systems under the presence of circularly polarized laser fields. Finally, our findings are summarized in section 4.

2. Method

Here we describe the simple but realistic theoretical modeling of massless and massive Dirac fermion systems. The systems are described by the following widely used Hamiltonian at each $\vec{k}$-point,

$$H_{\vec{k}} = \hbar v_{\mathrm{F}} \tau_z \sigma_x k_x + \hbar v_{\mathrm{F}} \sigma_y k_y + \frac{\Delta}{2}\sigma_z, \tag{1}$$

where $\sigma_{u=x,y,z}$ is a Pauli matrix, v_{F} is the Fermi velocity, and Δ is the band gap of the system. If Δ is set to zero, the system corresponds to a massless Dirac fermion system. Otherwise, the system is a massive Dirac fermion system. The chirality of the system is given by $\tau_z = \pm 1$. Note that the positive and negative chiralities correspond to the Dirac cone of graphene at K and K' points, respectively. Thus, one needs to include both contributions in the simulation to accurately describe the low energy states of graphene. In this work, we fix the Fermi velocity v_{F} to 1.12×10^6 m s^{-1}, which corresponds to that of graphene computed by the *ab initio* calculation [40].

To describe the light-driven electron dynamics in massive and massless Dirac fermion systems with dissipation, we employ the following quantum Liuoville equation for the reduced single-particle density matrix

$$\frac{\mathrm{d}}{\mathrm{d}t}\rho_{\vec{K}(t)}(t) = \frac{[H_{\vec{K}(t)}, \rho_{\vec{K}(t)}(t)]}{\mathrm{i}\hbar} + \hat{D}_{\vec{K}(t)}\rho_{\vec{K}(t)}(t), \tag{2}$$

with a time-dependent Hamiltonian $H_{\vec{K}(t)}$ and a phenomenological relaxation operator $\hat{D}_{\vec{K}(t)}$. The time-dependent Hamiltonian is given as

$$H_{\vec{K}(t)} = \hbar v_{\mathrm{F}} \tau_z \sigma_x K_x(t) + \hbar v_{\mathrm{F}} \sigma_y K_y(t) + \frac{\Delta}{2}\sigma_z, \tag{3}$$

where the light-matter coupling is described by the Peierls substitution, $\vec{K}(t) = \vec{k} + e\vec{A}(t)/\hbar c$, with a spatially uniform vector potential $\vec{A}(t)$.

We construct the relaxation operator $\hat{D}_{\vec{K}(t)}(t)$ based on the relaxation time approximation [41]. For this purpose, we first express the reduced density matrix $\rho_{\vec{K}(t)}(t)$ on the basis of Houston states [42, 43], which are

eigenstates of the instantaneous Hamiltonian $H_{\vec{K}(t)}$ at each instance; $H_{K(t)}|u^{\rm H}_{bk}(t)\rangle = \epsilon_{bK(t)}|u^{\rm H}_{bk}(t)\rangle$, where b denotes the band index, valence ($b = v$) or conduction ($b = c$) bands. The reduced density matrix can be expanded with the Houston states at each $\vec{k}$-point as

$$\rho_{\vec{K}(t)}(t) = \sum_{bb'} \rho_{bb',\vec{K}(t)} |u^{\rm H}_{b\vec{k}}(t)\rangle \langle u^{\rm H}_{b'\vec{k}}(t)|, \tag{4}$$

which can be written in matrix form with the Houston basis,

$$\rho_{\vec{K}(t)}(t) \coloneqq \begin{pmatrix} \rho_{vv,\vec{K}(t)}(t) & \rho_{vc,\vec{K}(t)}(t) \\ \rho_{cv,\vec{K}(t)}(t) & \rho_{cc,\vec{K}(t)}(t) \end{pmatrix}. \tag{5}$$

In the basis of the Houston states, we further construct the relaxation operator $\hat{D}_{\vec{K}(t)}$ with the phenomenological relaxation time, T_1 and T_2, as

$$\hat{D}_{\vec{K}(t)}\rho_{\vec{K}(t)} \coloneqq -\begin{pmatrix} \frac{\rho_{vv,\vec{K}(t)}(t) - \rho^{\rm eq}_{v\vec{K}(t)}}{T_1} & \frac{\rho_{vc,\vec{K}(t)}(t)}{T_2} \\ \frac{\rho_{cv,\vec{K}(t)}(t)}{T_2} & \frac{\rho_{cc,\vec{K}(t)}(t) - \rho^{\rm eq}_{c\vec{K}(t)}}{T_1} \end{pmatrix}, \tag{6}$$

where $\rho^{\rm eq}_{b\vec{K}(t)}$ is the Fermi–Dirac distribution,

$$\rho^{\rm eq}_{b,K(t)} = \frac{1}{{\rm e}^{(\epsilon_{bK(t)}-\mu)/k_{\rm B}T_e} + 1} \tag{7}$$

with the electron temperature T_e and the chemical potential μ_e. In this work, we fix the electron temperature to 80 K and the chemical potential to zero unless stated otherwise. Here, T_1 denotes the longitudinal relaxation time, which is responsible for the population decay, while T_2 denotes the transverse relaxation time, which is responsible for decoherence. According to [28], the relaxation times, T_1 and T_2, are set to 100 fs and 20 fs, respectively. Here, we choose the longitudinal relaxation time T_1 according to the electron thermalization time scale, while the transverse relaxation time T_2 according to the electron–electron scattering time scale [44–46].

Instead of the use of Houston states $|u^{\rm H}_{v\vec{k}}(t)\rangle$, one may consider to employ static Bloch states, which are eigenstates of the Hamiltonian, $H_{\vec{k}}|u^{\rm B}_{b\vec{k}}\rangle = \epsilon_{b\vec{k}}|u^{\rm B}_{b\vec{k}}\rangle$, to construct the dissipation operator. However, as will be shown later, the dissipation operator based on the Bloch states fails to describe fundamental properties of materials because the field-induced intraband motion is not taken into account in the Bloch basis.

Employing the time-evolving reduced density matrix $\rho_{\vec{K}(t)}(t)$, one can compute dynamics of a general one-body observable $\hat{O}$ as

$$\langle \hat{O}(t)\rangle = \frac{1}{(2\pi)^2}\int {\rm d}\vec{k}\ {\rm Tr}\,[\hat{O}\rho_{\vec{K}(t)}(t)]. \tag{8}$$

In this work, we focus on the transport property of massive and massless Dirac fermion systems. Thus, we compute the time-evolution of the electric current, employing the following current operator,

$$\hat{J}_i(t) = -\frac{c}{\hbar}\frac{\partial H_{\vec{K}(t)}}{\partial A_i}, \tag{9}$$

where A_i is the ith component of the vector potential $\vec{A}(t)$.

3. Results

3.1. Dissipation constructed with Houston and Bloch states

Here, we elucidate the two kinds of dissipation operators $\hat{D}$ to demonstrate that taking the appropriate basis for the density matrix is crucial: one is constructed with the Houston states, as explained in section 2. The other is constructed with the static Bloch states, which are eigenstates of the field-free Hamiltonian, instead of using the Houston states. For the sake of the investigation, we first evaluate the direct current (DC) transport property of a massless Dirac fermion system, i.e. a model for graphene.

To evaluate the DC transport property, we compute the electric current under a static source–drain field. To smoothly apply the source–drain field $\vec{E}_{\rm SD}(t)$, we employ the following time-profile that includes a switch-on process

$$\vec{E}_{\rm SD}(t) = E_{\rm SD}\vec{e}_x f\left(\frac{t}{T_{\rm switch}}\right), \tag{10}$$

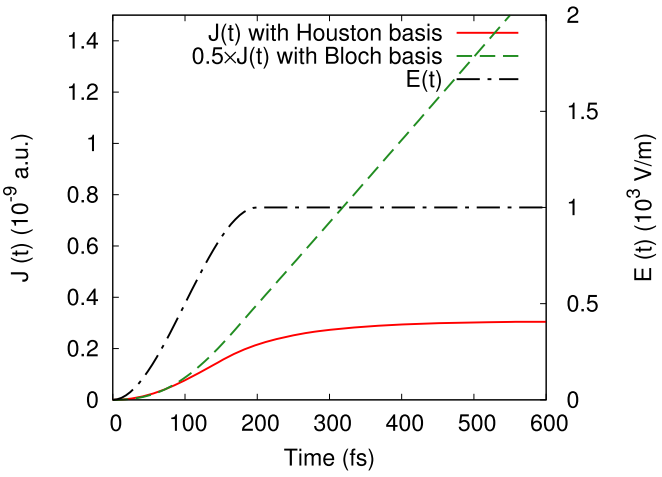

Figure 1. Current as a function of time in a massless Dirac fermion system under a weak quasi-static electric field. The red-solid line shows the result with the phenomenological dissipation constructed with the Houston basis, and the green-dashed line shows that constructed with the Bloch basis. The black dash–dot line shows the applied electric field (right axis).

where the switching function $f(x)$ is defined as

$$f(x) = \begin{cases} 1, & 1 < x \\ 3x^2 - 2x^3, & 0 < x \leqslant 1 \\ 0, & \text{otherwise.} \end{cases} \tag{11}$$

Here, we set the source–drain direction to the x-direction, the source–drain field strength E_{SD} to 10^3 V m^{-1}, and the switching time T_{switch} to 200 fs.

Figure 1 shows the computed current along the source–drain field direction as a function of time. The red-solid line shows the result employing the relaxation operator constructed with the Houston basis, while the green-dashed line shows that with the Bloch basis. The time-profile of the applied electric field is also shown as the black dash–dot line. One sees that the result using the Houston states (red-solid) converges to the constant current on the time scale of the relaxation. Therefore, the system reaches a nonequilibrium steady state under the presence of the source–drain field, and the saturated current can be described as a function of the applied field strength, $J(E_{\mathrm{SD}})$. In the weak field limit, the perturbative expansion can be applied, and one obtains $J(E_{\mathrm{SD}}) = \sigma E_{\mathrm{SD}}$. Indeed, we numerically confirmed that the current in figure 1 is already in this linear response regime. Thus, we can confirm that the dissipation operator constructed with the Houston states can naturally reproduce Ohm's law. On the other hand, the result using the Bloch states (green-dashed) monotonically increases and diverges in the long time propagation limit. This fact means that the system does not reach a steady state, demonstrating that the relaxation operator constructed with the Bloch states induces an artificial error, violating Ohm's law.

Next, we consider the Hall transport property with the dissipation constructed with the Houston and the Bloch states. For this purpose, we set the gap Δ to 100 meV, and the chirality τ_z to $+1$. All the other parameters are the same as for the above DC transport investigation with the massless Dirac fermion system. We compute the Hall current along the x-axis under the presence of the slowly-switched-on electric field along the y-axis. Here, we define the instantaneous Hall conductivity σ_{xy} as a ratio of the instantaneous Hall current and the strength of the source–drain field E_{SD}.

In figure 2, the red-solid line shows the result computed with the dissipation constructed with the Houston states, while the green-dashed line shows that with the Bloch states. As a reference, the blue-dotted line shows the result without any dissipation. The Hall conductivity without any dissipation converges to $-e^2/2h$ under the static electric field, showing the half integer of the quantized conductivity in agreement with the basic theory of anomalous Hall effect [47]. The Hall conductivity computed with relaxation in the Houston basis fairly reproduces the quantized conductivity, indicating that relaxation does not have any significant effect in the regime of adiabatic evolution. On the other hand, the Hall conductivity computed with relaxation based on the static Bloch basis significantly deviates from the quantized value, showing divergent behavior. Therefore, the relaxation operator constructed with the Bloch states fails to capture the transport property of a topological insulator.

The failure of the relaxation operator constructed with the static Bloch states can be understood in terms of the following unphysical excitation mechanism: under a static electric field, the vector potential $\vec{A}(t)$ monotonically increases and the Hamiltonian $H_{\vec{k}(t)}$ changes in time. If the system has a substantial gap, the

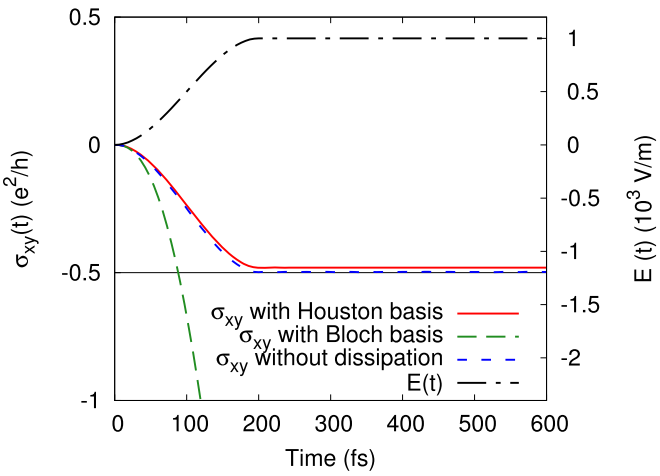

Figure 2. Hall conductivity as a function of time in a massive Dirac fermion system under a weak quasi-static electric field. The red-solid line shows the result with the phenomenological dissipation constructed with the Houston basis, the green-dashed line shows that constructed with the Bloch basis, and the blue-dotted line shows that without any dissipation. The black dash–dot line shows the applied electric field.

dynamics has to be adiabatic and the states have to be well approximated by the eigenstates of the instantaneous Hamiltonian. However, once the relaxation operator constructed with the static Bloch states is applied, the operator forces the system to remain in the initial Bloch states, which are not the eingenstates of the instantaneous Hamiltonian. Therefore, the relaxation operator using the Bloch states disturbs the adiabatic dynamics, and the system is artificially excited. This unphysical excitation appears as the diverging current in the DC transport of the massless Dirac fermion system (in figure 1) and in the Hall transport of the massive Dirac fermion system (in figure 2). In contrast, the Houston states can naturally capture this adiabatic dynamics since they are defined as instantaneous eigenstates of the Hamiltonian $H_{\vec{K}(t)}$. Therefore, the relaxation operator constructed with the Houston states does not disturb the adiabatic dynamics under a static electric field, and it can properly describes the dissipative property of dynamical systems.

Here we examined the properties of the relaxation operator constructed with the Houston states only for the quasi-static responses as shown in figures 1 and 2. However, importantly, we note that the same description of the relaxation has been recently examined even for time-dependent fields in both linear and nonlinear response regimes and has been demonstrated to fairly capture the experimentally observed features in the context of the energy loss spectroscopy and the high-order harmonic generation from solids [48, 49]. Thus, hereafter, we employ the relaxation operator constructed with the Houston states in order to investigate the light-induced Hall responses under the simultaneous presence of static and dynamical fields.

3.2. Light-induced Hall effect in graphene

Next, we investigate the anomalous Hall effect induced by circularly polarized light in a massless Dirac fermion system that models the Dirac bands in graphene. Figure 3 shows a schematic picture of our simulation setup that mimics the experimental setup of [27]. We compute the electron dynamics under the presence of circularly-polarized light and a static source–drain field, and we compute the Hall current, which is perpendicular to the source–drain direction.

To practically compute the light-induced Hall current, we employ the following form for a circular laser pulse,

$$\vec{A}_{\rm cir}(t) = -\frac{cE_{\rm cir}}{\omega_{\rm cir}}\left[\cos\left(\frac{\pi t}{T_{\rm cir}}\right)\right]^2 \times [\vec{e}_x \sin(\omega_{\rm cir} t) + \tau_{\rm cir}\vec{e}_y \cos(\omega_{\rm cir} t)] \quad (12)$$

in the domain $-T_{\rm cir}/2 < t < T_{\rm cir}/2$ and zero outside. Here, $\hbar\omega_{\rm cir}$ is the mean photon energy, $T_{\rm cir}$ is the full duration, $E_{\rm cir}$ is the maximum of the field strength of a circularly-polarized laser field. The chirality of the circular laser is given by $\tau_{\rm cir} = \pm 1$. According to previous work [28], we set the full width at half maximum of the pulse to 1 ps, the wavelength of the laser to 6.5 μm, which corresponds to the photon energy of $\hbar\omega_{\rm cir} \approx 190$ meV. For the source–drain field, we employ the form of equation (10), setting $E_{\rm SD}$ to 10^4 V m^{-1} and $T_{\rm SD}$ to 20 fs.

To make the direct connection to the experiment [27], we evaluate the light-induced Hall current as the difference of the transverse current induced by positive and negative chirality pump laser fields (pump dichroism). Figure 4(a) shows the field strength profile of a circular laser pulse and the source–drain field as

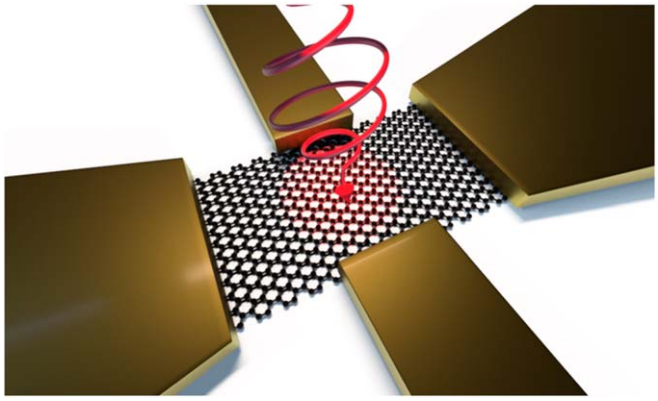

Figure 3. Schematic picture of the experimental setup for the light-induced anomalous Hall effect in graphene.

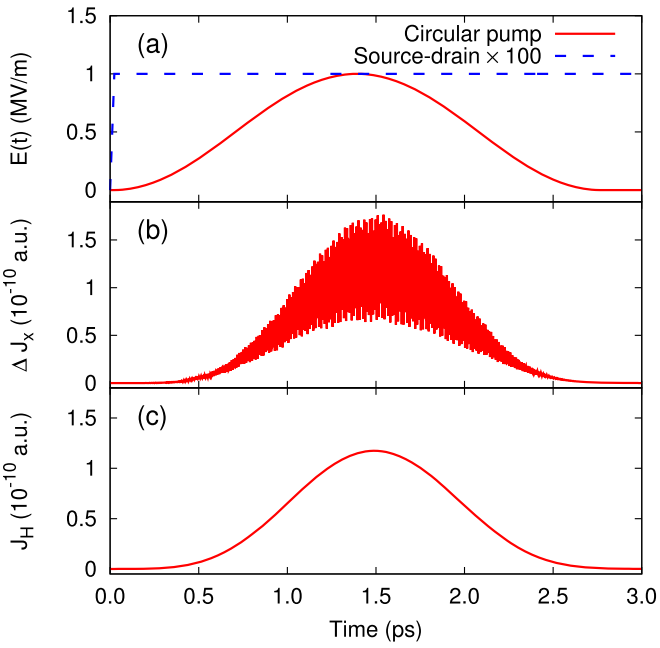

Figure 4. Evaluation of the light-induced Hall current in a massless Dirac fermion system. (a) The red-solid line shows the field strength of the circular laser pulse as a function of time, and the blue-dotted line shows that of the source–drain field. Here, the source–drain field (blue-dotted) is scaled by a factor of 100. (b) The difference of the transverse current induced by the positive and negative circularly polarized laser pulses. (c) The extracted Hall current evaluated by equation (13) with the transverse current in the panel (b).

functions of time, while figure 4(b) shows the difference of the transverse current $\Delta J(t)$ induced by the positive and negative circular laser pulses under the presence of the source–drain field. As seen from figure 4(b), the dichroism current $\Delta J(t)$ shows high-frequency components. These high-frequency components are not relevant for the transport property because there is no mean charge flow with the time-average. To extract the DC component of the transverse current, we define the Hall current as the temporal-average of the dichroism current as

$$J_{\rm H}(t) = \frac{1}{\sqrt{2\pi\sigma_W^2}} \int {\rm d}t' \Delta J(t') \exp\left[\frac{(t-t')^2}{2\sigma_W^2}\right], \tag{13}$$

where the width of the temporal average σ_W is set to 100 fs.

Figure 4(c) shows the computed Hall current $J_{\rm H}(t)$ as a function of time. One sees that the Hall current shows the similar profile to the applied circular field. This fact indicates that the light-induced Hall effect in the present conditions can be characterized with a quasi-steady-state due to the balance of the laser excitation and the relaxation at each instance. Indeed, it was demonstrated that the Hall conductivity evaluated with the peak Hall

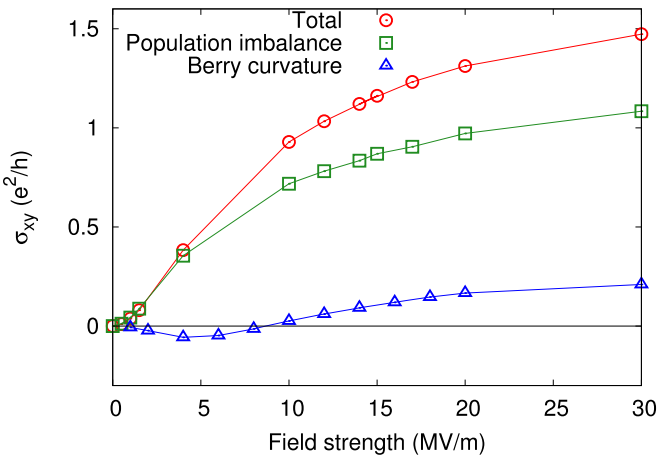

Figure 5. Light-induced Hall conductivity σ_{xy} as a function of the field strength of the applied circular laser field. The red circles show the total Hall conductivity computed with the total current operator, equation (9). The green squares show the contribution from the population imbalance computed with the intraband current, equation (14). The blue triangles show the contribution from the Berry curvature of natural orbitals computed with equation (20).

current induced by a circular laser pulse is well described by that evaluated with a steady state under the continuous circular laser [28].

Next, we investigate the light-induced Hall effect by changing the field strength of the circular laser pulses. For this purpose, we define the light-induced Hall conductivity σ_{xy} of the massless Dirac fermion system as the ratio of the peak Hall current $J_{\rm H}^{\rm peak}$ and the source–drain field strength $E_{\rm SD}$, $\sigma_{xy} = J_{\rm H}^{\rm peak}/E_{\rm SD}$.

In figure 5, the red circles show the computed Hall conductivity as a function of the applied circular laser fields. One sees that the Hall conductivity monotonically increases and shows a saturation behavior in the strong field regime. In the experiment, a similar saturation has been reported as the saturated conductivity of $\sigma_{xy}^{\rm exp} = 1.8 \pm 0.4e^2/h$ [27]. Therefore, our simulation provides a consistent result with previous experimental work.

In our previous theoretical work [28], it was demonstrated that the light-induced Hall effect in graphene dominantly originates from the population imbalance of photocarriers in the momentum space. Here, we revisit this interpretation from a different angle. For this purpose, we evaluate the contribution of the momentum-space population imbalance to the Hall current by the following intraband current

$$\vec{J}_{\rm intra}(t) = \frac{1}{(2\pi)^2}\sum_{b=v,c}\int {\rm d}\vec{k} n_{b\vec{K}(t)}\frac{\partial \epsilon_{b\vec{K}(t)}}{\partial \vec{k}}, \tag{14}$$

where $\vec{K}(t)$ is the accelerated Bloch wavevector, $\vec{K}(t) = \vec{k} + e\vec{A}(t)/\hbar c$, $\epsilon_{b\vec{k}}$ is the eigen-energy of the Dirac Hamiltonian at $\vec{k}$. Here, the instantaneous occupation $n_{b\vec{K}(t)}(t)$ is computed by the projection onto the Houston state as

$$n_{b\vec{K}(t)}(t) = {\rm Tr}\left[\rho_{K(t)}(t)|u_{b\vec{k}}^{\rm H}(t)\rangle\langle u_{b\vec{k}}^{\rm H}(t)|\right]. \tag{15}$$

Note that the intraband current in equation (14) is nothing but the current computed solely by the diagonal elements of the current operator in equation (9) in the Houston basis representation. Because the band velocity of the Dirac bands, $\partial\epsilon_{b\vec{k}}/\partial\vec{k} = \pm v_f\vec{k}/|\vec{k}|$, is isotropic around the Dirac point, the light-induced Hall current computed with equation (14) purely originates from the symmetry breaking of the photocarrier distribution $n_{b\vec{K}(t)}(t)$ in the Brillouin zone.

In figure 5, the green squares show the population imbalance contribution computed by equation (14). In the weak field regime, the population imbalance contribution of the bare Dirac bands well reproduces the total Hall conductivity (red circles). Therefore, the light-induced anomalous Hall effect dominantly originates from the population imbalance of photocarriers. Furthermore, even in the strong field regime, the population imbalance contribution fairly captures general trends of the total signal. Therefore, the population imbalance picture is still relevant even in the strong field regime.

To obtain further insight into microscopic physics behind the light-induced anomalous Hall effect, we investigate a property of steady states under the presence of circularly-polarized light. For this purpose, we numerically construct a steady state by solving equation (2) under the presence of a continuous circularly-polarized laser field without the static source–drain field. After the long time propagation, the system reaches a steady state due to the balance of the laser excitation and the relaxation. The single-particle density matrix of such steady state has a periodicity in time, $\rho_{\vec{K}(t)}(t) = \rho_{\vec{K}(t)}(t + T_{\rm cycle})$, with the period of the external field $T_{\rm cycle}$.

To investigate details of such steady state density matrix, we consider the expansion with natural orbitals [50] as

$$\rho_{\vec{K}(t)}(t) = \sum_b n^{\mathrm{NO}}_{b\vec{k}}(t)|u^{\mathrm{NO}}_{b\vec{k}}(t)\rangle\langle u^{\mathrm{NO}}_{b\vec{k}}(t)|, \tag{16}$$

where $|u^{\mathrm{NO}}_{b\vec{k}}(t)$ is a natural orbital, and $n^{\mathrm{NO}}_{b\vec{k}}(t)$ is the occupation of the natural orbital. Thanks to the time periodicity of the density matrix, the natural orbitals may have the same time periodicity as $|u^{\mathrm{NO}}_{b\vec{k}}(t + T_{\mathrm{cycle}})\rangle = |u^{\mathrm{NO}}_{b\vec{k}}(t)\rangle$.

Importantly, the expectation value of single-particle operators, equation (8), can be expressed as a sum of the expectation value of each natural orbital with the occupation weight as,

$$\langle\hat{O}(t)\rangle = \frac{1}{(2\pi)^2}\int \mathrm{d}\vec{k}\sum_b n^{\mathrm{NO}}_{b\vec{k}}(t)\langle u^{\mathrm{NO}}_{b\vec{k}}(t)|\ \hat{O}|u^{\mathrm{NO}}_{b\vec{k}}(t)\rangle. \tag{17}$$

Therefore, the natural orbital is one of the most suitable descriptors of the system in a single-particle picture. Based on this fact, we investigate properties of the steady states with their natural orbitals.

As seen in figure 5, the contribution from the population imbalance in the bare Dirac bands (green-square) dominates the total conductivity (red-circle) in the weak field regime. Therefore, the steady state in the weak field regime is expected to be well characterized by the valence and conduction states of the bare Dirac bands. Once the field strength becomes strong, the contribution from the population imbalance mechanism shows a discrepancy from the total conductivity. Thus, in the strong field regime, the bare valence and conduction states would not be suitable descriptors of the system anymore. In order to access this hypothesis, we introduce a measure of similarity of the natural orbitals and the Houston states (the instantaneous eigenstates of the Hamiltonian). We shall call it *Houston fidelity*. To define the Houston fidelity, we first introduce a fidelity matrix $F^{\mathrm{H}}_{\vec{k}}$ at each $\vec{k}$ such that each matrix element $F_{ij,\vec{k}}$ is the cycle-average of the squared overlap of the ith natural orbital and the jth Houston state as

$$F_{ij,\vec{k}} = \frac{1}{T_{\mathrm{cycle}}}\int_0^{T_{\mathrm{cycle}}} \mathrm{d}t\ |\langle u^{\mathrm{NO}}_{i\vec{k}}(t)|u^{\mathrm{H}}_{j\vec{k}}(t)\rangle|^2. \tag{18}$$

Then, the Houston fidelity is defined as the absolute value of the determinant of the fidelity matrix, $S^{\mathrm{H}}_{\vec{k}} = |\det F_{\vec{k}}|$. Note that the Houston fidelity, $S^{\mathrm{H}}_{\vec{k}}$, takes the maximum value of one only if the natural orbitals are identical to the Houston states at all the time. In general, $0 \leqslant S^{\mathrm{H}}_{\vec{k}} \leqslant 1$.

In contrast to the above bare band picture, one may consider a photon-dressed band picture based on the Floquet theory. Under the continuous laser driving, the Hamiltonian $H(t)$ has the time periodicity with the period of T_{cycle}. Then, a Floquet state $u^{\mathrm{F}}_{b\vec{k}}(t)$ may be introduced as a part of a solution of the time-dependent Schrödinger equation with a time-periodic Hamiltonian

$$\mathrm{i}\hbar\frac{\mathrm{d}}{\mathrm{d}t}|\Psi^{\mathrm{F}}_{b\vec{k}}(t)\rangle = H_{\vec{K}(t)}|\Psi^{\mathrm{F}}_{b\vec{k}}(t)\rangle, \tag{19}$$

where the solution $|\Psi^{\mathrm{F}}_{b\vec{k}}(t)\rangle$ consists of the time periodic Floquet state, $|u^{\mathrm{F}}_{b\vec{k}}(t + T_{\mathrm{cycle}})\rangle = |u^{\mathrm{F}}_{b\vec{k}}(t)\rangle$, and a pure phase factor as $|\Psi^{\mathrm{F}}_{b\vec{k}}(t)\rangle = \exp[-\mathrm{i}\epsilon^{\mathrm{F}}_{b\vec{k}}t]|u^{\mathrm{F}}_{b\vec{k}}(t)\rangle$. Here, $\epsilon^{\mathrm{F}}_{b\vec{k}}$ is the Floquet quasienergy. One may further introduce a measure of similarity of the natural orbitals and the Floquet states by employing the Floquet states in equation (18) instead of the Houston states. This was introduced as $S^{\mathrm{F}}_{\vec{k}}$ *Floquet fidelity* in previous work [28], and it was used to demonstrate that the Floquet states are realized in graphene under the presence of a strong laser field.

Since photocarriers are expected to play a significant role in the light-induced anomalous Hall effect, we now investigate the steady state density matrix at a resonant k-point where the vertical gap is identical to the photon energy, $|k| = \hbar\omega_{\mathrm{cir}}/2v_{\mathrm{F}}$. Figure 6(a) shows the Houston fidelity $S^{\mathrm{H}}_{\vec{k}}$ and the Floquet fidelity $S^{\mathrm{F}}_{\vec{k}}$ at the resonant k-point as a function of field strength of the circular laser field. In the weak field regime, the Houston fidelity is close to one, indicating that the steady state is well characterized by the bare Dirac bands. As the field strength becomes stronger, the Houston fidelity monotonically decreases, indicating that the states are significantly dressed by photons and the system is not well characterized by the bare Dirac bands anymore. These findings fairly support the above hypothesis. The Floquet fidelity $S^{\mathrm{F}}_{\vec{k}}$ at the resonance in figure 6(a) is close to zero in the weak field regime. This fact indicates that the photon-dressing electronic state is significantly disturbed by the dissipation, and the Floquet states cannot be formed in the weak field regime. Once the field strength increases, the photon-dressing effect becomes more significant and overcomes the dissipation effects. As a result of the competition of the dressing and the dissipation, the Floquet states can be fairly well formed in a strong field regime. However, once the field strength becomes stronger than 20 MV m^{-1}, the Floquet fidelity starts decreasing. This fact can be understood by the opening of additional dissipative channels due to the significant intraband motion of electrons in the Brillouin zone: Once the field strength becomes strong enough, the momentum shift of the electron $e|\vec{A}(t)|/\hbar c$ becomes comparable to the distance between the Dirac point and

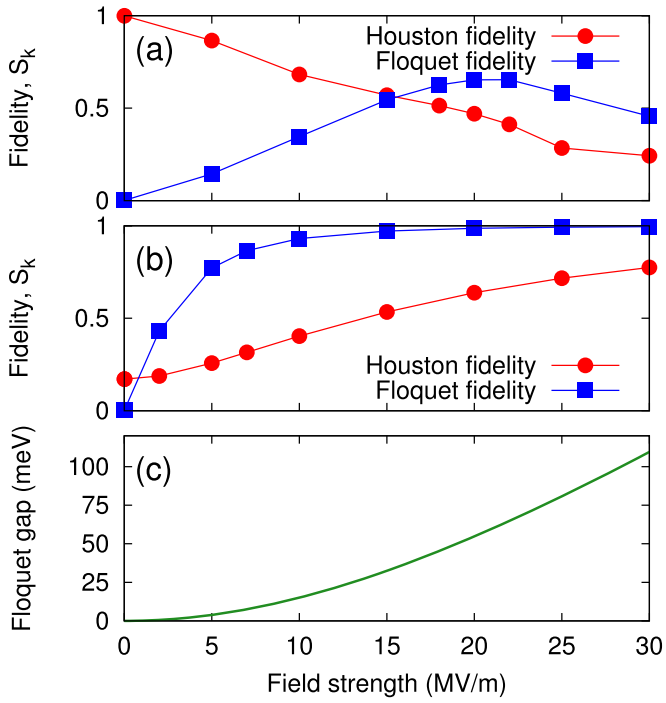

Figure 6. Calculated Houston fidelity $S_{\vec{k}}^{\mathrm{H}}$ and Floquet fidelity $S_{\vec{k}}^{\mathrm{F}}$ (see main text for details) as functions of field strength at (a) the resonant k-point, $|k| = \hbar\omega_{\mathrm{cir}}/2v_f$ and (b) the Dirac point, $\vec{k} = 0$. (c) The Floquet gap at the Dirac point as a function of field strength of the circular laser field.

the resonant k-point $|k| = \hbar\omega_{\mathrm{cir}}/2v_{\mathrm{F}}$. As a result, electrons that originally stay around the resonant point can move around the Dirac point, where the gap between the conduction and valence states is small. Because of the small gap nature, additional dissipative channels can be opened, and the photon-dressing effect is significantly disturbed. Indeed, the momentum shift corresponding to the field strength of 30 MV m^{-1} is about 8.3×10^{-3} a.u., and it exceeds the resonant momentum $|k| = \hbar\omega_{\mathrm{cir}}/2v_{\mathrm{F}} = 6.8 \times 10^{-3}$ a.u.

Next, we investigate the steady state density matrix at the Dirac point instead of the resonance. Figure 6(b) shows the Houston fidelity $S_{\vec{k}}^{\mathrm{H}}$ and the Floquet fidelity $S_{b\vec{k}}^{\mathrm{F}}$ at the Dirac point, $\vec{k} = 0$. In contrast to the result at the resonance, the Houston fidelity is much smaller than one even in the weak field limit. This fact indicates that the bare band picture is significantly disturbed by the weak external driving because of the gapless feature at the Dirac point. The Floquet fidelity at the Dirac point is almost zero in the weak field limit, while it quickly converges to one as the field strength increases. Therefore, the Floquet states are well established at the Dirac point in the strong field regime. This fact is consistent with the above finding in the resonance condition: the Floquet states are significantly disturbed by the dissipation in the weak field regime, while they are stabilized in the strong field regime because the photon-dressing effect overcomes the dissipation effect. One sees that the Houston fidelity seems to converge to one in the strong field limit, indicating that the adiabatic picture becomes suitable in the strong field regime. However, the realization of the adiabatic states requires much higher field strength, compared with the Floquet states.

Based on the Floquet picture, it was demonstrated that the Floquet quasienergy shows the band-gap opening at the Dirac point under the presence of a circularly-polarized laser field, and the Floquet states show the emergence of Berry curvatures [18]. Furthermore, the light-induced anomalous Hall effect was predicted based on the anomalous velocity due to the Floquet Berry curvature. Figure 6(c) shows the Floquet gap at the Dirac point as a function of the field strength of the circular laser field. The gap reaches 100 meV at the highest field strength, 30 MV m^{-1}. According to figure 6(b), one expects that, in the strong field regime, the system forms the Floquet states and shows the Floquet Berry curvature contribution to the Hall effect due to the topological gap opening. Indeed, it was demonstrated that the natural orbitals of the non-equilibrium steady state with dissipation show Berry curvatures consistent with those of the Floquet states [28]. To quantify the Berry curvature contribution to the light-induced anomalous Hall effect, we extend the expression of the Hall conductivity with the Floquet states [18] to that with the natural orbitals as

$$\sigma_{xy}^{\mathrm{B}} = \frac{2e^2}{\hbar}\int\frac{\mathrm{d}\vec{k}}{(2\pi)^2}\sum_b \tilde{n}_{b\vec{k}}^{\mathrm{NO}}\tilde{\Omega}_{b\vec{k}}^{\mathrm{NO}}, \tag{20}$$

where $\tilde{n}_{b\vec{k}}^{\mathrm{NO}}$ is the cycle-average natural orbital occupation, and $\tilde{\Omega}_{b\vec{k}}^{\mathrm{NO}}$ is the cycle-averaged Berry curvature of natural orbitals defined as

$$\tilde{\Omega}_{b\vec{k}}^{\mathrm{NO}} = -\mathrm{i}\frac{1}{T_{\mathrm{cycle}}}\int_0^{T_{\mathrm{cycle}}}\mathrm{d}t\,\vec{\nabla}_{\vec{k}}\times\langle u_{b\vec{k}}^{\mathrm{NO}}(t)|\vec{\nabla}|\,u_{b\vec{k}}^{\mathrm{NO}}(t)\rangle. \tag{21}$$

In figure 5, the blue triangles show the Berry curvature contribution to the light-induced Hall conductivity computed with equation (20). One sees that the light-induced Berry curvature shows non-zero contribution to the light-induced Hall conductivity. However, it is a rather minor contribution compared with the population imbalance effect. Therefore, we can conclude that the light-induced anomalous Hall effect in graphene dominantly originates from the photocarrier population imbalance in momentum space.

3.3. Light-induced Hall effect in topological insulators

In the previous section, we discussed the emergent Berry curvature contribution to the light-induced anomalous Hall effect in the massless Dirac fermion system. Here, we investigate the Hall transport properties of a system where the light-induced extrinsic contributions coexist with the intrinsic topological contribution. For this purpose, we investigate the light-induced anomalous Hall effect in a massive Dirac fermion system. We set the gap Δ to 100 meV, which is comparable to the Flouqet gap of the massless Dirac fermion system at the highest field strength (see figure 6(c)). The other parameters are the same as the previous massless Dirac fermion system.

In order to investigate the relation between the chirality of light (τ_{cir}) and the intrinsic chirality of the system (τ_z), we do not employ the pump dichroism but employ the cycle-averaged current of a nonequilibrium steady state under the presence of the source–drain field and a continuous circular laser field, fixing the chirality of light to positive ($\tau_{\mathrm{cir}} = +1$).

Figure 7(a) shows the computed Hall conductivity σ_{xy} as a function of field strength of the circular laser field. The red circles show the conductivity of the positive chirality system ($\tau_z = +1$), while the blue squares show that of the negative chirality system ($\tau_z = -1$). In the weak field limit, the two systems show the intrinsic Hall conductivities with the opposite sign, reflecting the intrinsic Berry curvature contribution. Once the field strength becomes strong, the two systems with the different chiralities start showing qualitatively different behaviors because they have opposite intrinsic contributions and a common extrinsic contribution. The positive chirality system ($\tau_z = +1$) shows negative conductivity in the weak field limit. As the field strength increases, the absolute value of the conductivity decreases. When the field strength reaches around 8 MV m^{-1}, the Hall conductivity becomes zero due to the cancellation of the intrinsic and extrinsic contributions. Once the field strength becomes stronger, the conductivity changes its sign to positive and monotonically increases. On the other hand, the negative chirality system ($\tau_z = -1$) does not show the sign change in the Hall conductivity. Interestingly, the conductivities of the two systems converge to a similar value in the strong field regime. These facts indicate that the common extrinsic contribution to the Hall transport property overcomes the intrinsic Berry curvature contribution in the strong field regime.

In order to elucidate the microscopic mechanism of the Hall transport property of the massive Dirac fermion system in the presence of the circular laser field, we evaluate the contribution from the population imbalance of photocarriers with equation (14) and the Berry curvature contribution by equation (20).

Figure 7(b) shows the result of the positive chirality system ($\tau_z = +1$). Here, in the weak field limit, the total conductivity (red circle) shows the half integer of the quantized conductivity $-0.5e^2/h$ due to the intrinsic topological contribution, and this value is well described by the natural-orbital Berry curvature contribution (blue triangle). Thus, we can confirm that the intrinsic Berry curvature contribution is well captured by the natural orbital expression, equation (20). Furthermore, since there is no photocarrier generation in the weak field limit, the contribution from the population imbalance (green square) is zero in this regime. As the field strength increases, the Berry curvature contribution becomes smaller while the population imbalance starts being the larger contribution in the positive chiral system. As a result, the sign of the Hall conductivity changes from negative to positive. This fact indicates the robustness of the extrinsic population contribution and a possibility that the intrinsic property of the system can be completely overwritten by the extrinsic property with the strong optical driving.

Figure 7(c) shows the result of the negative chirality system ($\tau_z = -1$). In contrast to the positive chirality system, the Hall conductivity of the negative chirality system shows the positive conductivity in the weak field regime. Furthermore, the Hall conductivity does not show the sign change even in the strong field regime. This behavior can be understood by the fact that, in the negative chirality system, the intrinsic and the extrinsic contributions have the same sign in the Hall conductivity (see figure 7(c)). In figure 7(c), while the Berry curvature contribution (blue triangle) dominates the intrinsic Hall transport property in the weak field limit, it is

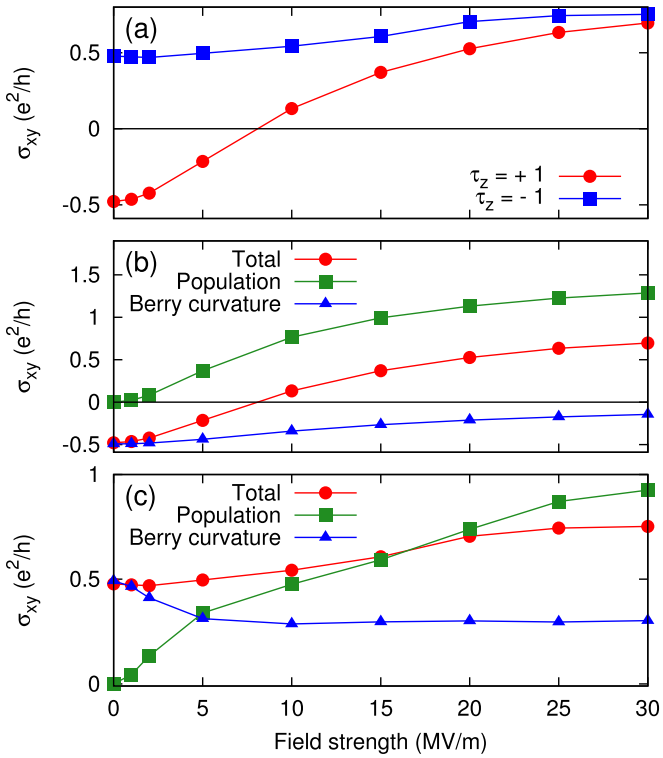

Figure 7. Hall conductivities as a function of the field strength of the applied circular laser fields. (a) The total Hall conductivity of the massive Dirac fermion system is shown for the positive chirality system ($\tau_z = +1$) as the red circles and for the negative chirality system ($\tau_z = -1$) as the blue squares. (b) The Hall conductivity of the positive chirality system is shown. The red circles show the total conductivity, the green squares show the contribution from the population imbalance computed with equation (14), and the blue triangles show the Berry curvature contribution computed by equation (20). (c) shows now the Hall conductivity for the negative chirality system.

weakened once the field strength becomes strong. On the other hand, while the contribution from the population imbalance is negligible in the weak field regime, it becomes significant in the strong field regime. Therefore, in both positive and negative chirality systems, the intrinsic topological contribution is weakened by the laser driving, while the light-induced extrinsic contribution dominates the total Hall transport property.

Finally, we investigate the effect of electron (hole) doping on the anomalous Hall effect in the massive Dirac fermion system. In previous theoretical and experimental works, the doping effect on the light-induced anomalous Hall effect in graphene has been investigated [27, 28], and it was demonstrated that the light-induced Hall conductivity in the strong field regime shows a double-peak structure with a central plateau as a function of the chemical potential. Here, we elucidate the role of the intrinsic Hall transport property in the optically-driven massive Dirac fermion system with electron (hole) doping.

Figure 8(a) shows the Hall conductivities of the massive Dirac fermion systems in equilibrium without optical driving as a function of chemical potential μ, while figure 8(b) shows those under the presence of the strong circular laser field ($E_{\rm cir} = 20$ MV m^{-1}). In equilibrium, the conductivities show the central plateau region the width of which is comparable with the size of the gap $\Delta = 100$ meV. Depending on the chirality of the system ($\tau_z = \pm 1$), the Hall conductivity has the opposite sign. In contrast, in the nonequilibrium steady state under the presence of the strong laser field, the Hall conductivities become positive regardless of the chirality of the system. Furthermore, both chiral systems show the common feature; the double peak structure with the central plateau region. This feature is consistent with the emergent feature of the light-induced anomalous Hall effect in graphene. These findings indicate that, although the systems with opposite chiralities have significantly different intrinsic properties in equilibrium, the properties can be overwritten by the strong optical drive.

4. Summary

In this work, we investigated the transport property of massless and massive Dirac fermion systems that mimic graphene and topological insulators, respectively. Dirac fermion systems under the coexistence of light and

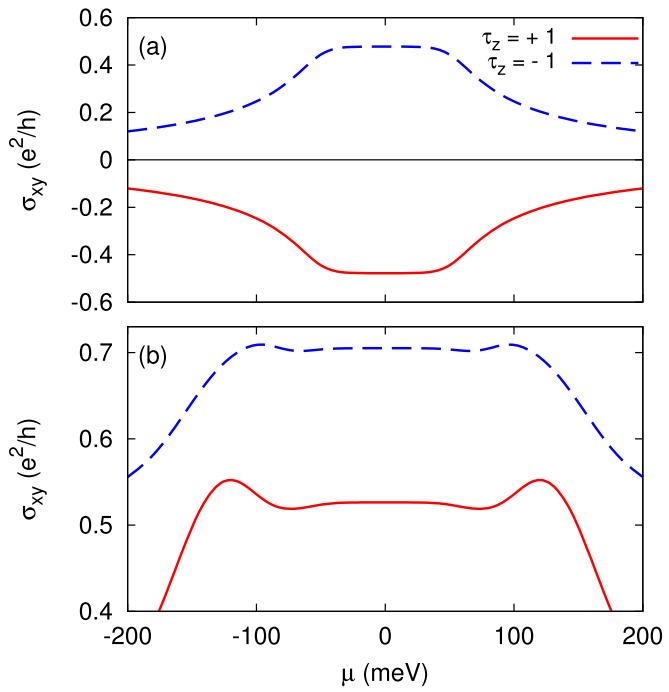

Figure 8. Hall conductivities of the massive Dirac fermion systems as a function of chemical potential μ. (a) The Hall conductivities in equilibrium without optical-driving are shown for the positive chirality system ($\tau_z = +1$) as the red-solid line and for the negative chirality system ($\tau_z = -1$) as the blue-dashed line. (b) The Hall conductivities in a non-equilibrium steady state with the optical driving ($E_{\rm cir} = 20$ MV m^{-1}) are shown.

dissipation in order to provide the microscopic insight into the dynamics of optically-driven nonequilibrium systems.

We assessed two kinds of phenomenological relaxation operators: one is constructed with the Houston states, which are the instantaneous eigenstates of Hamiltonian. The other is constructed with the static Bloch states, which are static eigenstates of the field-free Hamiltonian. It was demonstrated that the relaxation operator constructed with the Houston states satisfies Ohm's low for a metallic system and reproduces the quantized Hall conductivity of a topological insulator while the relaxation operator constructed with the Bloch states fails to satisfy Ohm's low and to reproduce the quantized conductivity, showing divergence of the current. The failure of this relaxation operator can be understood by an artificial excitation via the relaxation operator because the field-induced intraband motion is not properly taken into account, which is instead naturally included in the operator using the Houston states. Thus, the Houston state expression is indispensable to properly construct the dissipation operator and to be able to address the dynamical simulation of the driven system.

We then investigated the light-induced anomalous Hall effect in a massless Dirac fermion system that mimics the Dirac bands of graphene. We demonstrated that the massless Dirac fermion system shows the Hall transport property under the presence of circular laser fields. Based on the microscopic analysis, we clarified that the imbalance of photocarrier distribution in the Brillouin zone is the main origin of the light-induced Hall transport property although the nonzero light-induced Berry curvature contribution was also found. We further analyzed the steady-state density matrix under the continuous circular laser driving. As a result, we found that the Floquet states are not well formed in the weak field regime due to dissipation while they are well formed in the strong field regime because the photon-dressing overcomes the dissipation effect.

Next, we studied the Hall transport property of the massive Dirac fermion system under the presence of the circular laser fields in order to investigate the interplay of the intrinsic and the extrinsic contributions to the Hall transport. In the weak field regime, the intrinsic topological contribution dominates the Hall transport property while the photocarrier population effect is negligible. Once the field strength becomes strong, the topological contribution becomes weakened while the photocarrier population effect becomes significant. Surprisingly, if the intrinsic and the extrinsic contributions have opposite signs to the Hall conductivity, the sing of the Hall conductivity of the topological insulator can be flipped by the strong laser driving. Note that, in addition to the intrinsic Berry curvature contribution, it is known that extrinsic scattering processes such as the skew-scattering may have a significant contribution to the anomalous Hall effect in equilibrium phases [51]. Because the scattering processes depend much on population distributions of carriers, the photocarrier effect investigated in this work may further modify the extrinsic scattering contribution and open yet another possibility of

controlling Hall transport properties by light. This possibility will be investigated by integrating the corresponding scattering mechanisms into the present model in future work.

The above findings demonstrate the robustness and the generality of the photocarrier population imbalance effect in the optically-driven nonequilibrium systems. Importantly, we demonstrated that the extrinsic population effect can overwrite intrinsic properties of materials. Therefore, the population control can be a key to realize the optical control of material properties. Furthermore, by combining the population control with the state control such as the Floquet engineering by photon-dressing, properties and functionalities of materials can be largely controlled via light and novel features in nonequilibrium systems may be discovered.

Acknowledgments

We acknowledge fruitful discussions with J W McIver, G Jotzu, and A Cavalleri. This work was supported by the European Research Council (ERC-2015-AdG694097). The Flatiron Institute is a division of the Simons Foundation. SAS gratefully acknowledges the fellowship from the Alexander von Humboldt Foundation. MAS acknowledges financial support by the DFG through the Emmy Noether programme (SE 2558/2-1). PT acknowledges the received funding from the European Unions Horizon 2020 research and innovation programme under the Marie Sklodowska-Curie grant agreement No 793609. AR acknowledges support from the Cluster of Excellence 'Advanced Imaging of Matter' (AIM).

ORCID iDs

S A Sato https://orcid.org/0000-0001-9543-2620
M A Sentef https://orcid.org/0000-0002-7946-0282
U De Giovannini https://orcid.org/0000-0002-4899-1304
H Hübener https://orcid.org/0000-0003-0105-1427
A Rubio https://orcid.org/0000-0003-2060-3151

References

[1] Krausz F and Stockman M I 2014 *Nat. Photon.* **8** 205
[2] Basov D N, Averitt R D and Hsieh D 2017 *Nat. Mater.* **16** 1077
[3] Fausti D, Tobey R I, Dean N, Kaiser S, Dienst A, Hoffmann M C, Pyon S, Takayama T, Takagi H and Cavalleri A 2011 *Science* **331** 189–91
[4] Mitrano M *et al* 2016 *Nature* **530** 461
[5] Shin D, Hübener H, De Giovannini U, Jin H, Rubio A and Park N 2018 *Nat. Commun.* **9** 638
[6] Mentink J H, Balzer K and Eckstein M 2015 *Nat. Commun.* **6** 6708
[7] Tancogne-Dejean N, Sentef M A and Rubio A 2018 *Phys. Rev. Lett.* **121** 097402
[8] Sentef M A, Ruggenthaler M and Rubio A 2018 *Sci. Adv.* **4** eaau6969
[9] Topp G E, Tancogne-Dejean N, Kemper A F, Rubio A and Sentef M A 2018 *Nat. Commun.* **9** 4452
[10] Golez D, Eckstein M and Werner P 2019 arXiv:1903.08713 [cond-mat]
[11] Kennes D M, Claassen M, Sentef M A and Karrasch C 2019 *Phys. Rev.* B **100** 075115
[12] Ruggenthaler M, Tancogne-Dejean N, Flick J, Appel H and Rubio A 2018 *Nat. Rev. Chem.* **2** 0118
[13] Claassen M, Kennes D M, Zingl M, Sentef M A and Rubio A 2019 *Nat. Phys.* **15** 766–70
[14] Schultze M *et al* 2014 *Science* **346** 1348–52
[15] Lucchini M, Sato S A, Ludwig A, Herrmann J, Volkov M, Kasmi L, Shinohara Y, Yabana K, Gallmann L and Keller U 2016 *Science* **353** 916–9
[16] Mashiko H, Oguri K, Yamaguchi T, Suda A and Gotoh H 2016 *Nat. Phys.* **12** 741
[17] Schlaepfer F, Lucchini M, Sato S A, Volkov M, Kasmi L, Hartmann N, Rubio A, Gallmann L and Keller U 2018 *Nat. Phys.* **14** 560–4
[18] Oka T and Aoki H 2009 *Phys. Rev.* B **79** 081406
[19] Kitagawa T, Oka T, Brataas A, Fu L and Demler E 2011 *Phys. Rev.* B **84** 235108
[20] Lindner N H, Refael G and Galitski V 2011 *Nat. Phys.* **7** 490
[21] Ezawa M 2013 *Phys. Rev. Lett.* **110** 026603
[22] Sentef M A, Claassen M, Kemper A F, Moritz B, Oka T, Freericks J K and Devereaux T P 2015 *Nat. Commun.* **6** 7047
[23] Mikami T, Kitamura S, Yasuda K, Tsuji N, Oka T and Aoki H 2016 *Phys. Rev.* B **93** 144307
[24] Hübener H, Sentef M A, De Giovannini U, Kemper A F and Rubio A 2017 *Nat. Commun.* **8** 13940
[25] Haldane F D M 1988 *Phys. Rev. Lett.* **61** 2015–8
[26] Wang X, Ronca E and Sentef M A 2019 *Phys. Rev.* B **99** 235156
[27] McIver J W, Schulte B, Stein F U, Matsuyama T, Jotzu G, Meier G and Cavalleri A 2018 arXiv:1811.03522
[28] Sato S A *et al* 2019 *Phys. Rev.* B **99** 214302
[29] Foa Torres L E F, Perez-Piskunow P M, Balseiro C A and Usaj G 2014 *Phys. Rev. Lett.* **113** 266801
[30] Chan C K, Lee P A, Burch K S, Han J H and Ran Y 2016 *Phys. Rev. Lett.* **116** 026805
[31] Chan C K, Oh Y T, Han J H and Lee P A 2016 *Phys. Rev.* B **94** 121106
[32] Yan Z and Wang Z 2016 *Phys. Rev. Lett.* **117** 087402
[33] Ezawa M 2017 *Phys. Rev.* B **96** 041205
[34] Liu Y, Yang S A and Zhang F 2018 *Phys. Rev.* B **97** 035153

[35] Dehghani H, Oka T and Mitra A 2014 *Phys. Rev.* B **90** 195429
[36] Seetharam K I, Bardyn C E, Lindner N H, Rudner M S and Refael G 2015 *Phys. Rev.* X **5** 041050
[37] Abanin D, De Roeck W, Ho W W and Huveneers F 2017 *Commun. Math. Phys.* **354** 809–27
[38] Weidinger S A and Knap M 2017 *Sci. Rep.* **7** 45382
[39] Schüler M, Budich J C and Werner P 2019 *Phys. Rev.* B **100** 041101(R)
[40] Trevisanutto P E, Giorgetti C, Reining L, Ladisa M and Olevano V 2008 *Phys. Rev. Lett.* **101** 226405
[41] Meier T, von Plessen G, Thomas P and Koch S W 1994 *Phys. Rev. Lett.* **73** 902–5
[42] Houston W V 1940 *Phys. Rev.* **57** 184–6
[43] Krieger J B and Iafrate G J 1986 *Phys. Rev.* B **33** 5494–500
[44] Breusing M, Kuehn S, Winzer T, Malić E, Milde F, Severin N, Rabe J P, Ropers C, Knorr A and Elsaesser T 2011 *Phys. Rev.* B **83** 153410
[45] Brida D *et al* 2013 *Nat. Commun.* **4** 1987
[46] Gierz I *et al* 2015 *Phys. Rev. Lett.* **115** 086803
[47] Xiao D, Chang M C and Niu Q 2010 *Rev. Mod. Phys.* **82** 1959–2007
[48] Floss I, Lemell C, Wachter G, Smejkal V, Sato S A, Tong X M, Yabana K and Burgdörfer J 2018 *Phys. Rev.* A **97** 011401
[49] Floss I, Lemell C, Yabana K and Burgdörfer J 2019 *Phys. Rev.* B **99** 224301
[50] Löwdin P O 1955 *Phys. Rev.* **97** 1474–89
[51] Nagaosa N, Sinova J, Onoda S, MacDonald A H and Ong N P 2010 *Rev. Mod. Phys.* **82** 1539–92